Dalton Transactions

PAPER

A cascade reaction: ring-opening insertion of dioxaphospholane into lutetium alkyl bonds†

Cite this: DOI: 10.1039/c3dt52790e

Kevin R. D. Johnson and Paul G. Hayes*

Received 7th October 2013,
Accepted 26th November 2013

DOI: 10.1039/c3dt52790e

www.rsc.org/dalton

Geometrically constrained dioxaphospholane rings were incorporated into a bis(phosphinimine)carbazole ligand (H**L**) in an effort to generate an ancillary ligand system that is capable of supporting reactive lutetium alkyl functionalities and resistant to cyclometalation reactivity. This new ligand was used to prepare a lutetium dialkyl species, **L**Lu(CH_2SiMe_3)$_2$; however, the complex exhibited low thermal stability at ambient temperature. This dialkyl compound was found to be highly susceptible to a cascading inter- and intramolecular reaction that resulted in the sole formation of an asymmetric bimetallic tetraalkoxide complex. The product of this reaction, generated by the ring-opening insertion of dioxaphospholane moieties into lutetium–carbon bonds, was characterized by multinuclear NMR spectroscopy and single crystal X-ray diffraction.

Introduction

In research investigating structural properties and reactivity of the rare earth metals, a recent popular trend has been the development of non-carbocyclic ligands for use in supporting highly reactive complexes.[1–3] A diverse array of new ligand scaffolds has arisen throughout this "post-metallocene era" allowing for the synthesis of metal complexes that possess a wide variety of steric and electronic environments. Through the development of rare earth complexes supported by non-carbocyclic ligands, various new platforms for obtaining rare bonding motifs have also been witnessed. For example, recent use of a PNP pincer ligand has led to the isolation of a stable lutetium phosphinidene complex,[4] while a modified β-diketiminate ancillary has been used to isolate a terminal scandium imido species.[5–8]

Of particular interest to us is the development of non-carbocyclic ancillary ligands that possess phosphinimine functionalities and their subsequent application in rare earth chemistry. The P═N moiety is useful from a synthetic standpoint due to its strong donor properties, thermal robustness, modularity, and ability to be studied with $^{31}P\{^1H\}$ NMR spectroscopy. A variety of phosphinimine-containing ligands have previously been reported as supporting ancillaries for rare earth metals and selected frameworks are depicted in Chart 1. Featured ligands include the bis(phosphinimine)methane (i),[9–13] amino-phosphinimine (ii),[14–16] anilido-phosphinimine (iii),[17–20] phosphazene (iv),[21] bis(phosphinimine)carbazole (v),[22,23] bis(phosphinimine)pyrrole (vi),[24] and phosphasalen (vii)[25,26] scaffolds. This diverse set of ancillaries offers a variety of chelation geometries, steric environments and electronic properties, which in turn can allow for the development of rare bonding motifs, unique reaction behaviour and improved catalytic activity.

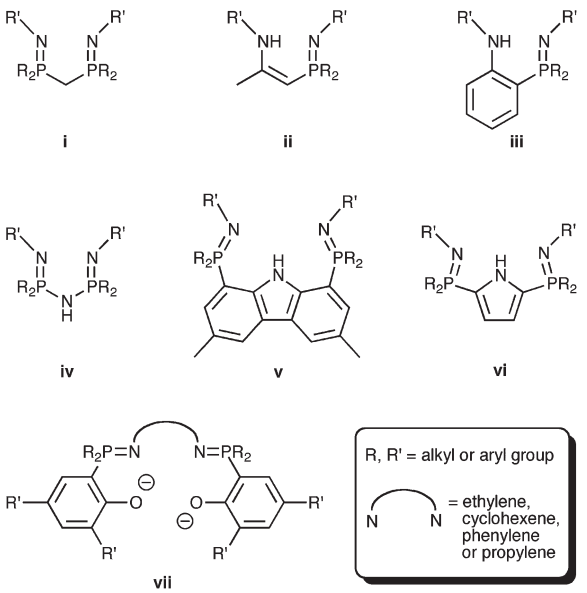

Chart 1 Selected phosphinimine ligands.

In our attempts to study reaction behaviour in rare earth metal complexes, we initially focused our attention on the

Department of Chemistry and Biochemistry, University of Lethbridge, 4401 University Drive, Lethbridge, AB T1 K 3M4, Canada. E-mail: p.hayes@uleth.ca; Fax: +1 403 329 2057; Tel: +1 403 329 2313

†CCDC 953674 (**5**), 953675 (**6**) and 953676 (**8**). For crystallographic data in CIF or other electronic format see DOI: 10.1039/c3dt52790e

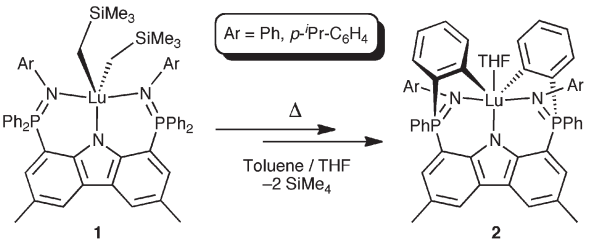

Scheme 1 Sequential double cyclometalation of **1**.

bis(phosphinimine)carbazole scaffold (**v**, R = Ph, R′ = Ph or 4-^{i}Pr-C$_6$H$_4$), due to its rigid aromatic backbone and monoanionic charge. Our initial investigations with this ligand involved the preparation of dialkyl lutetium complexes (**1**), however, these species were found to be highly thermally reactive at ambient temperature and, as a result, susceptible to rapid intramolecular metalative C–H bond activation processes with concomitant loss of alkane. The result of these sequential reactions were lutetium complexes that were coordinated by the ligand in a κ^5 manner, *via* three nitrogen atoms and two *ortho*-metalated P-phenyl rings (**2**, Scheme 1).[22] Similar *ortho*-metalation reactivity has been described with various other rare earth complexes supported by phosphinimine ligands.[27] Additionally, there is precedent for metalative C–H bond activation to occur even upon replacement of phosphinimine P-phenyl rings with less bulky methyl groups bound to phosphorus.[20]

To address this phosphinimine metalation issue, a potentially viable solution that we are pursuing involves linking the R groups on phosphorus together. The intention of this approach is to generate a phosphorous-containing ring with a constrained geometry so as to raise the energy barrier for the requisite highly ordered σ-bond metathesis transition state, thereby rendering metalative C–H bond activation less feasible. To this end, we have begun investigations into various phosphorus-containing ring systems and their capacity to restrict cyclometalation when installed onto our bis(phosphinimine)-carbazole framework. Specifically, the five membered phospholane and dioxaphospholane rings were considered for this purpose. While both phospholane and dioxaphospholane groups are geometrically constrained, the dioxaphospholane ring possesses oxygen atoms in the α-position to phosphorus, thus eliminating potential for C–H bond activation at those sites. Furthermore, the oxygen atoms were considered to be potential Lewis basic donors, should it prove possible for the ring to pivot to within close proximity of the metal centre. Finally, the dioxaphospholane group is commercially available in the form of 2-chloro-1,3,2-dioxaphospholane as an inexpensive reagent for use in our multi-step ligand synthesis (*vide infra*). Conversely, the oxygen-free analogue chlorophospholane is not commercially available and its preparation requires multiple synthetic steps and is low yielding.[28,29] For these reasons, dioxaphospholane rings rather than phospholane groups appeared to be a more attractive system for our initial attempts to prepare a geometrically constrained bis(phosphinimine) ancillary. Herein, we report dioxaphospholane incorporation into the bis(phosphinimine)carbazole ligand framework and the potential of this new ligand to support organometallic rare earth species.

Results and discussion

Synthesis and characterization

In former derivatives of the bis(phosphinimine)carbazole ancillary, the phosphinimine functionality has been comprised of two phenyl rings attached to phosphorus, and an aryl ring (phenyl, *para*-isopropylphenyl or pyrimidine) bound to nitrogen. Using a similar synthetic protocol to that previously reported, the targeted bis(phosphinimine)carbazole ligand containing dioxaphospholane moieties was readily synthesized over three steps from 1,8-dibromo-3,6-dimethyl-9-^{t}BOC-carbazolide, **3**, as outlined in Scheme 2. It should be noted that access to reagent **3** from commercially available carbazole requires four synthetic steps which have been previously described.[22,30,31] Dioxaphospholane rings were first installed onto the carbazole framework by lithiation of **3** with four equiv. of ^{t}BuLi in diethyl ether followed by addition of 2.2 equiv. of 2-chloro-1,3,2-dioxaphospholane to generate the ^{t}BOC-protected derivative, **4**. Thermal deprotection of **4** at 160 °C liberated the desired bis(dioxaphospholane), **5** over 1.5 h. Finally, the phosphinimine functionality was assembled *via* a Staudinger reaction between **5** and *para*-isopropylphenyl azide (Pipp azide) with concomitant loss of N_2 to afford **6** in 45.2% overall yield.

The $^{31}P\{^{1}H\}$ NMR resonances (benzene-d_6) of **4** and **5** at δ 148.7 and 167.9, respectively were observed relatively far downfield, similar to that of the starting material 2-chloro-1,3,2-dioxaphospholane (δ 168.5, benzene-d_6). However, upon oxidation of the phosphorus centres, a substantial upfield shift in the $^{31}P\{^{1}H\}$ NMR resonance of **6** was observed (δ 24.2, benzene-d_6).

In order to gain insight into the structure of the dioxaphospholane ring when attached to the dimethylcarbazole

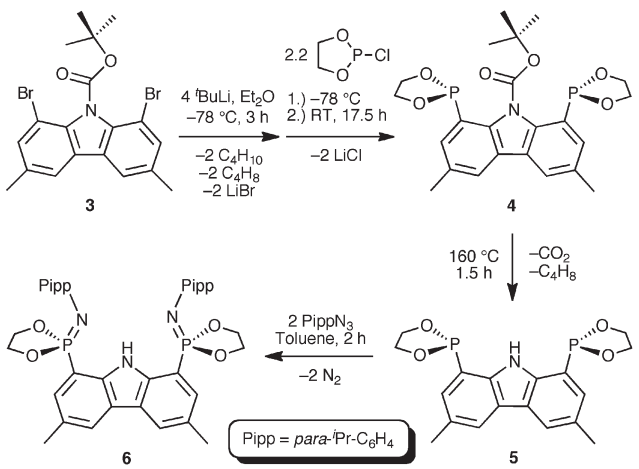

Scheme 2 Synthesis of pincer ligand **6**.

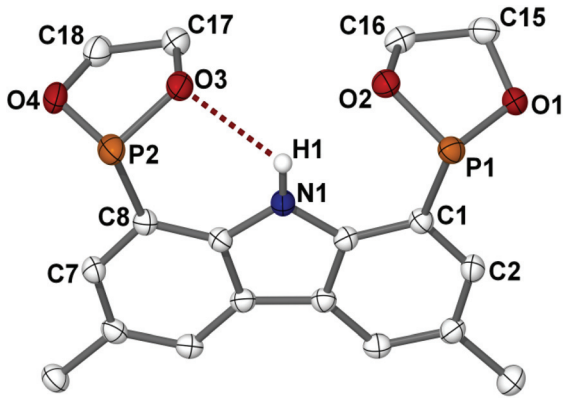

Fig. 1 Thermal ellipsoid plot (50% probability) of **5** with hydrogen atoms (except H1), omitted for clarity.

backbone, single crystal X-ray diffraction experiments were performed on compounds **5** and **6**. Of particular relevance is an investigation into the extent to which the dioxaphospholane ring could pivot about the C–P bond; this information is key to qualitatively assessing the conformational influence that this geometrically constrained ring has on the structure of the ancillary ligand.

Recrystallization of **5** from a concentrated pentane solution at ambient temperature afforded single crystals that were suitable for an X-ray diffraction experiment. The bis(dioxaphospholane) compound crystallized in the space group $P\bar{1}$ and the molecular structure is depicted in Fig. 1 as a thermal ellipsoid plot. In the solid-state structure, both dioxaphospholane rings are pivoted so that they are perpendicular to the face of the planar dimethylcarbazole backbone (O2–P1–C1–C2 torsion angle of 152.0(2)° and O3–P2–C8–C7 torsion angle of −155.2(2)°). This particular conformation of the two dioxaphospholane moieties can be attributed to two factors: (i) a hydrogen bonding interaction can occur between an oxygen atom of the dioxaphospholane ring and the carbazole proton. The distance between the donor and acceptor atoms in the N1–H1···O3 interaction in **5** is 2.857(2) Å. A similar contact can also occur *via* O2, whereby the donor–acceptor distance for the N1–H1···O2 interaction has been determined to be 2.877(2) Å. (ii) This orientation also allows for energetically favourable aromatic π–π stacking interactions between the carbazole ring systems of two adjacent molecules of **5** in the solid state. This packing arrangement is depicted in Fig. 2.

A comparison of the metrical parameters of each dioxaphospholane ring in the molecule revealed slight variations in the P–O bond distances. In one ring, the P1–O2 distance is marginally longer at 1.643(1) Å, compared to the P1–O1 length of 1.635(1) Å. This is also the case for the other ring, whereby the P2–O3 distance (1.640(1) Å), is slightly elongated compared to the P2–O4 contact of 1.628(2) Å. This difference in bond lengths for P1–O2 and P2–O3 may be a result of the fact that O2 and O3 are involved in hydrogen bonding to H1.

Recrystallization of protio ligand **6** from a concentrated benzene solution layered with pentane at ambient temperature

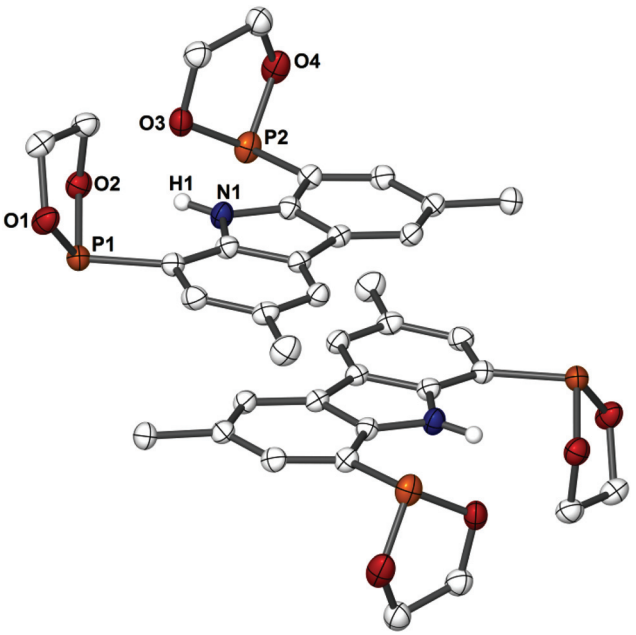

Fig. 2 Packing diagram of **5** with hydrogen atoms (except H1), omitted for clarity.

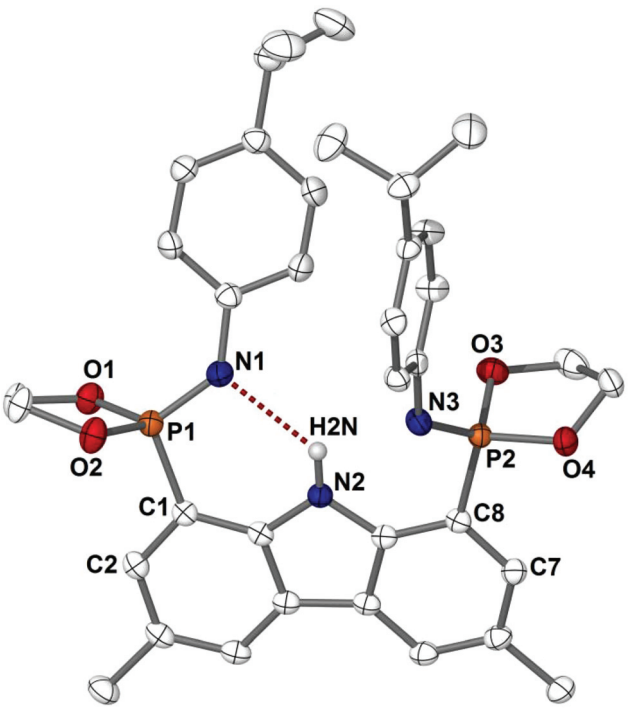

Fig. 3 Thermal ellipsoid plot (50% probability) of **6** with hydrogen atoms (except H2N), omitted for clarity.

afforded colourless prisms that were suitable for X-ray diffraction. The ancillary ligand crystallized in the orthorhombic space group *Pbca* (#61) and the molecular structure is depicted in Fig. 3 as a thermal displacement plot. The solid-state structure of **6** adopts a conformation whereby one phosphinimine

arm (N1–P1) is held periplanar to the dimethylcarbazole backbone (N1–P1–C1–C2 torsion angle of −165.2(1)°) and the other (N3–P2) is rotated further out of the aromatic plane (N3–P2–C8–C7 torsion angle of −140.8(1)°). The alignment of the N1–P1 phosphinimine group with the planar carbazole backbone is influenced by a hydrogen bond contact between N1 of the phosphinimine and the carbazole N–H (d(N···N) = 2.817(2) Å). In **6**, the N–P bond distance of the phosphinimine functionality was measured to be 1.535(1) Å for N1–P1 and 1.534(1) Å for N3–P2. This phosphinimine distance is consistent with the expected double bond character.[22,24,32]

Each phosphorus atom in the protio ligand exhibits roughly tetrahedral geometry. Of particular interest are the O–P–O bond angles of 96.34(6)° and 96.66(6)° for O1–P1–O2, and O3–P2–O4, respectively. Both of these angles are smaller than the average tetrahedral angle at phosphorus (avg = 109.32° for P1 and P2), and from this it can be inferred that the nature of the dioxaphospholane rings indeed constrain the oxygen atoms to the peripheral edge of the ligand. As such, the solid-state geometry of **6** suggests that when the ligand is coordinated in a tridentate mode to a metal *via* N1, N2, and N3, the dioxaphospholane moiety will be held significantly away from the metal centre on the condition that the tetrahedral bond angles at phosphorus persist. This described geometry is ideal for our purposes of designing a ligand that is resistant to cyclometalation *via* the PR_2 groups.

Ring-opening insertion reactivity

The protio ligand was readily complexed with lutetium *via* the alkane elimination reaction of **6** with $Lu(CH_2SiMe_3)_3(THF)_2$ (Scheme 3). *In situ* observation of the reaction in benzene-d_6 solution revealed the rapid formation of dialkyl complex **7** at ambient temperature with concurrent loss of one equivalent of $SiMe_4$ and two equivalents of THF. Unfortunately, **7** was found to be thermally reactive and rapidly decomposed to a new product; consequently, the dialkyl lutetium complex could not be isolated as a solid (Table 1).

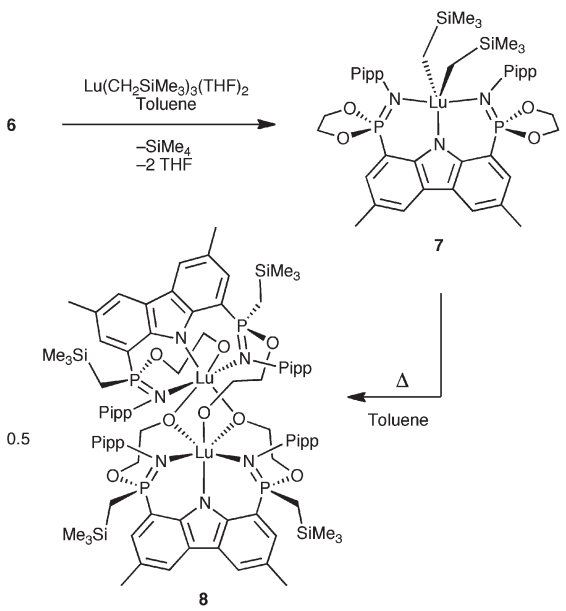

Scheme 3 Synthesis of **8** by dioxaphospholane ring-opening insertion.

Table 1 Selected bond distances (Å), angles (°), and torsion angles (°) for compounds **5** and **6**

	5	**6**
P1–O1	1.635(1)	1.600(1)
P1–O2	1.643(1)	1.606(1)
P2–O3	1.640(1)	1.609(1)
P2–O4	1.628(2)	1.600(1)
C1–P1	1.839(2)	1.777(2)
C8–P2	1.829(2)	1.778(2)
N1···O2[a]	2.877(2)	—
N1···O3[a]	2.857(2)	—
N1–P1[b]	—	1.535(1)
N3–P2[b]	—	1.534(1)
N2···N1[b]	—	2.817(2)
N2···N3[b]	—	3.049(2)
O1–P1–O2	95.47(7)	96.34(6)
O3–P2–O4	94.56(7)	96.66(6)
C1–P1–O2	100.66(8)	107.78(7)
C1–P1–O1	101.35(8)	107.43(7)
C8–P2–O3	100.56(8)	108.32(6)
C8–P2–O4	101.84(8)	106.98(6)
C1–P1–N1[b]	—	106.86(7)
C8–P2–N3[b]	—	108.14(7)
C2–C1–P1–O2	152.0(2)	66.4(1)
C2–C1–P1–O1	54.2(2)	−36.5(1)
C7–C8–P2–O3	−155.2(2)	91.6(1)
C7–C8–P2–O4	−58.2(2)	−11.6(1)
C2–C1–P1–N1[b]	—	−165.2(1)
C7–C8–P2–N3[b]	—	−140.8(1)

Notes: [a] The listed parameter pertains only to complex **5**. [b] The listed parameter pertains only to complex **6**.

Complete multinuclear NMR characterization of **7** at low temperature (−10 °C) in toluene-d_8 was attempted; however, even at reduced temperature, the spectra were found to be consistently contaminated with signals arising from reaction intermediates and the final decomposition product, resulting in ambiguous peak assignments. A similar result was observed when the reaction was performed at −78 °C. To a large degree, the NMR resonances corresponding to the final decomposition product (*vide infra*) could be subtracted from the spectra of **7**, allowing for fair confidence in ^{1}H and $^{31}P\{^1H\}$ NMR assignments. Unfortunately, this process was not suitable for assigning $^{13}C\{^1H\}$ NMR signals for **7**, due to the extreme complexity of the spectrum. In the $^{31}P\{^1H\}$ NMR spectrum (benzene-d_6) of **7**, a downfield shift was observed from that of the free protio ligand to δ 56.2. The expected methylene and $SiMe_3$ signals were observed in the ^{1}H NMR spectrum (benzene-d_6) at δ −0.28 and 0.24, respectively.

When the thermal decomposition of complex **7** was followed *in situ* at ambient temperature in benzene-d_6 solution, the $^{31}P\{^1H\}$ NMR spectrum revealed the initial formation of four new signals with equal integrations and a decrease in the dialkyl resonance. Likewise, the ^{1}H NMR spectrum (benzene-d_6) also displayed four sets of new signals with equal intensity

growing in place of those for **7**. Particularly evident in the ^{1}H NMR spectrum was the presence of four new $SiMe_3$ signals at δ −0.17, −0.21, −0.40, and −0.56 and four carbazole methyl resonances at δ 2.60, 2.51, 2.47 and 2.42. After 18 h at ambient temperature, conversion of **7** to a new product (**8**) was complete. Alternatively, heating a solution of **7** to 100 °C for 80 min allowed for rapid synthesis of the decomposition product **8**.

While it was evident from the NMR spectra that **8** was an asymmetric bimetallic complex, its identity could not initially be assigned with confidence. The presence of four $SiMe_3$ signals in the ^{1}H NMR spectrum and the lack of tetramethylsilane formation as a decomposition byproduct suggested that the thermal reactivity of **7** did not involve a cyclometalative alkane elimination mechanism (as previously observed for **1**). Particularly perplexing, however, was the fact that while four $SiMe_3$ signals were observed slightly upfield of 0 ppm in the ^{1}H NMR spectrum, there was no evidence of methylene resonances in that region of the spectrum, as would be expected for a complex containing Lu–CH_2SiMe_3 groups. Rather, various methylene signals were observed further downfield as a series of overlapping multiplets between δ 4.7–3.2 and δ 2.0–1.4.

Analysis of complex **8** by a DEPT-135 NMR experiment revealed twelve different methylene signals, eight of which could be categorized as –OCH_2– moieties, and four as –CH_2SiMe_3 groups (Fig. 4). Of the eight –OCH_2– methylene signals, five were split into doublets by J_{CP} spin–spin coupling of varying magnitudes. Four of the five exhibited coupling constants between 7 and 11 Hz, suggesting 2-bond coupling between carbon and phosphorus; while the fifth displayed a smaller coupling constant of 5 Hz, indicative of longer range (3-bond) coupling. All four signals corresponding to the methylene carbon atoms were split into doublets by J_{CP} coupling. Interestingly, the –CH_2SiMe_3 methylene doublets all exhibited very large J values between 84 and 93 Hz, which was suggestive of 1-bond coupling between carbon and phosphorus. On these grounds, the methylene signals in the spectrum were consistent with a compound that contained four inequivalent PCH_2SiMe_3 moieties and four $POCH_2CH_2O$– chains.

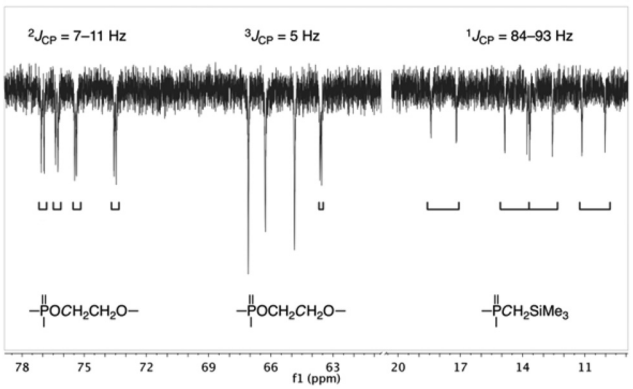

Fig. 4 Methylene regions in the DEPT-135 NMR spectrum of **8**.

From the described NMR data, it was premised that the structure of complex **8** was likely the product of a ring-opening insertion reaction of the ligand dioxaphospholane rings into the Lu–C bonds of **7**. Accordingly, the expected structure would contain trimethylsilylmethyl groups bound to phosphorus and ethylene glycoxide moieties connecting lutetium to a phosphorus atom of the ligand. The product of this reaction is depicted in Scheme 3 as an asymmetric bimetallic complex.

In order to unambiguously determine the structure of decomposition product **8**, a single crystal X-ray diffraction experiment was performed. Single crystals suitable for diffraction analysis were obtained from a concentrated benzene solution layered with pentane and the resulting molecular structure is depicted in Fig. 5 as a thermal displacement plot. As suggested by the NMR spectroscopic data, the solid-state structure of **8** was found to be an asymmetric bimetallic complex with one trimethylsilylmethyl group bound to each phosphorus atom in addition to ethylene glycoxide moieties linking each phosphorus atom to a lutetium metal centre. A unique structural feature of this bimetallic complex is that the two subunits are held together through Lewis acid–base interactions *via* the bridging alkoxy groups (O6 and O8), as well as by an anionic ligand-to-metal bonding interaction

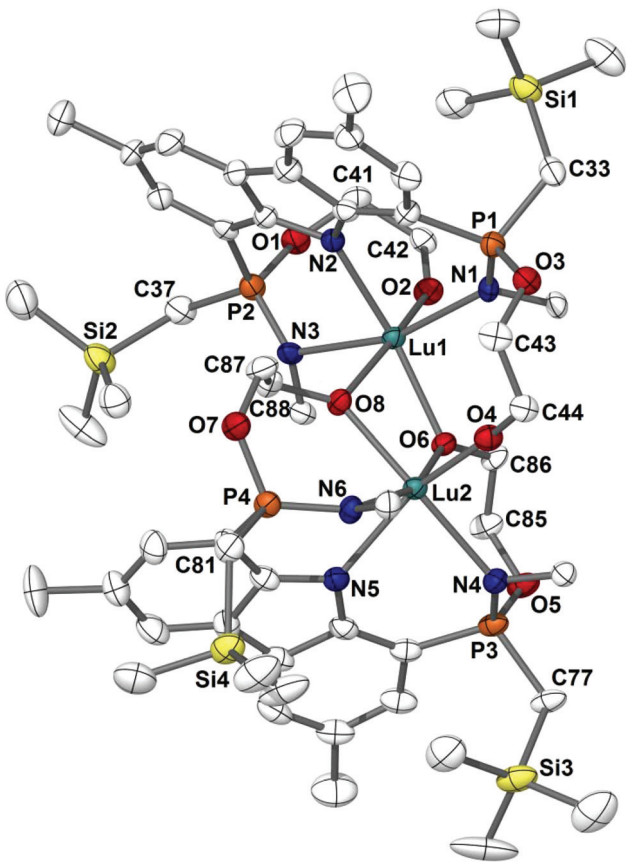

Fig. 5 Thermal ellipsoid plot (50% probability) of complex **8** with hydrogen atoms and *para*-isopropylphenyl rings (except for *ipso* carbons) omitted for clarity.

Table 2 Selected bond distances (Å) and angles (°) for complex **8**

Lu1–N1	2.338(4)	Lu2–N4	2.378(4)
Lu1–N2	2.362(4)	Lu2–N5	2.359(4)
Lu1–N3	2.387(4)	Lu2–N6	2.424(4)
Lu1–O2	2.061(3)	Lu2–O4	2.026(4)
Lu1–O6	2.229(3)	Lu2–O6	2.245(3)
Lu1–O8	2.286(3)	Lu2–O8	2.208(3)
P1–N1	1.583(4)	P3–N4	1.592(5)
P2–N3	1.583(4)	P4–N6	1.581(4)
Lu1–O6–Lu2	104.3(1)	Lu1–O8–Lu2	103.6(1)
O6–Lu1–N2	155.4(1)	N4–Lu2–O8	157.8(1)
N3–Lu1–N1	163.6(1)	N5–Lu2–O4	156.6(1)
O2–Lu1–O8	168.0(1)	N6–Lu2–O6	160.9(1)

whereby an ethylene glycoxide group from one subunit is tethered to the other subunit through the O4–Lu2 bond. As expected, the bridging lutetium alkoxide bonds are longer (2.229(3) Å, 2.245(3) Å, 2.286(3) Å, and 2.208(3) Å for Lu1–O6, Lu2–O6, Lu1–O8, and Lu2–O8, respectively) than the terminal lutetium alkoxide distances (2.061(3) Å and 2.026(4) Å for Lu1–O2 and Lu2–O4, respectively). The complex exhibits typical bond angles of 104.3(1)° and 103.6(1)° for the bridging Lu1–O6–Lu2 and Lu1–O8–Lu2 interactions, respectively.

In complex **8**, each lutetium centre exhibits distorted octahedral geometry with three sites occupied by alkoxide moieties and the remaining coordination sites defined by the nitrogen atoms of the ancillary ligand. Interestingly, the pincer ligand that is chelated to Lu1 adopts a meridional geometry about the metal *via* N1, N2 and N3, while a facial geometry is enforced at Lu2 as a result of the unique coordination mode of N4, N5 and N6 to the metal. The facial coordination mode of the ligand at Lu2 is somewhat surprising considering that the pincer design of the ancillary ligand was intended to enforce solely a meridional geometry at the metal centre (Table 2).

Mechanistic considerations

The ring-opening insertion reactivity that led to the formation of **8** is the first example, to the best of our knowledge, of a lanthanide alkyl cleaving a phosphonimidate ester P–O bond, although comparable reactivity has previously been documented in early transition metal chemistry. For example, a titanium benzyne species was reported to cleave a P–O bond of trimethylphosphite to afford a titanium aryl/alkoxide product.[33] Likewise, the reaction of trialkylphosphites with group 1 and group 2 organometallic reagents is an analogous transformation. In the generation of complex **8**, the mechanism presumably proceeds by coordination of an oxygen atom of the dioxaphospholane ring to a second lutetium centre, followed by ring-opening insertion *via* a four-centred transition state. This process could be repeated a total of four times, either in parallel or sequentially, to afford the final product (Scheme 4).

Conclusions

In an effort to modify the bis(phosphinimine)carbazole ligand so as to make it resistant to cyclometalation decomposition pathways, cyclic dioxaphospholane rings were installed at the PR_2 site affording a new protio ligand, **6**. A dialkyl lutetium complex of the ligand was prepared; however, it was susceptible to degradation *via* an unusual ring-opening insertion reaction. This decomposition route appears to have proceeded by an intra- and inter-molecular cascade involving the insertion reaction of four dioxaphospholane rings into four Lu–alkyl bonds to give the final "ring-opened" lutetium alkoxide bimetallic complex **8**. Notably, this was the first example of a lanthanide alkyl cleaving a phosphonimidate ester bond in this manner. While the cyclic, constrained geometry of the dioxaphospholane rings on the pincer ligand seemed well suited toward the restriction of cyclometalation reactions at the PR_2 sites, the presence of labile phosphonimidate ester P–O bonds caused detrimental effects. Due to the high reactivity of lutetium alkyl bonds with the phosphonimidate ester functionality of the dioxaphospholane rings, ligand **6** appears to be unsuitable for our purpose of stabilizing lanthanide alkyl complexes. However, research into an oxygen-free phospholane analogue to **6** as a "cyclometalation resistant" pincer ligand is currently underway in our laboratory. In the absence of reactive phosphonimidate ester P–O bonds, it is expected that this ancillary ligand should be capable of supporting highly reactive organolanthanide complexes.

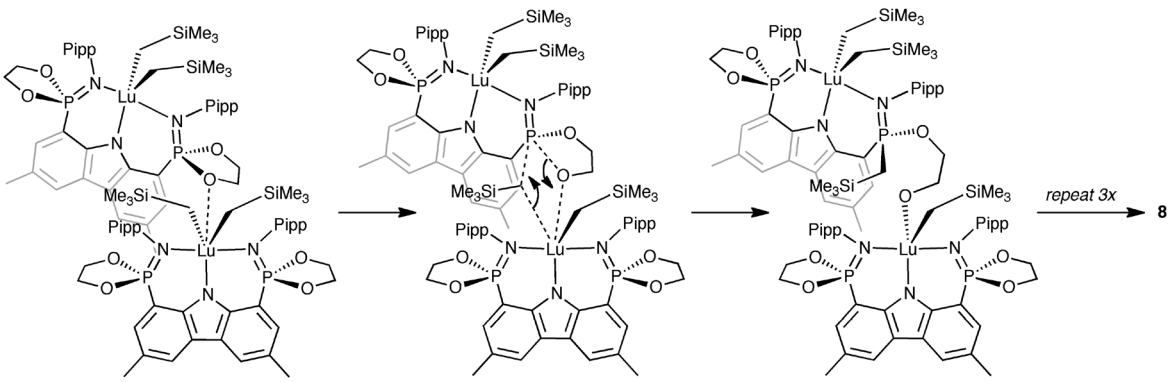

Scheme 4 Possible mechanism for dioxaphospholane ring-opening insertion.

Experimental

General procedures

Unless otherwise specified, all reactions were carried out under an argon atmosphere with the rigorous exclusion of oxygen and water using standard glove box (MBraun) or high vacuum line techniques. The solvents diethyl ether, pentane and toluene were dried and purified using a solvent purification system (MBraun) and stored in evacuated 500 mL bombs over sodium benzophenone ketyl (diethyl ether) or "titanocene" indicator (pentane and toluene). Deuterated solvents were dried over sodium benzophenone ketyl (benzene-d_6 and toluene-d_8) or calcium hydride (chloroform-*d*, dichloromethane-d_2), degassed *via* three freeze–pump–thaw cycles, distilled under vacuum and stored in glass bombs under argon. Unless otherwise specified, all solvents required for air-sensitive manipulations were introduced directly into the reaction flasks by vacuum transfer with condensation at −78 °C. Samples for NMR spectroscopy were recorded on a 300 MHz Bruker Avance II (Ultrashield) spectrometer (^{1}H 300.13 MHz, ^{13}C{^{1}H} 75.47 MHz, ^{31}P{^{1}H} 121.49 MHz) and referenced relative to either $SiMe_4$ through the residual solvent resonance(s) for ^{1}H and ^{13}C{^{1}H}; or external 85% H_3PO_4 for ^{31}P{^{1}H}. All NMR spectra were recorded at ambient temperature (25 °C) unless specified otherwise. Elemental analyses were performed using an Elementar Americas Vario MicroCube instrument. The reagent 2-chloro-1,3,2-dioxaphospholane was purchased from TCI America and used as received. The precursors $Lu(CH_2SiMe_3)_3(THF)_2$,[4,34–36] **3**,[22] and *para*-isopropylphenyl azide[22] were prepared according to literature procedures. All deuterated solvents were purchased from Cambridge Isotope Laboratories. All other reagents were obtained from Aldrich Chemicals or Alfa Aesar and used as received.

Synthesis of 4

A 2-neck round-bottomed flask was charged with **3** (3.06 g, 6.76 mmol, 1 equiv.) and 60 mL of diethyl ether to give a pale yellow-beige coloured suspension. The flask was cooled to −78 °C and a pentane solution (1.63 M) of *t*-BuLi (17.0 mL, 27.7 mmol, 4.1 equiv.) was added dropwise. Following the addition, the reaction mixture was stirred at −78 °C for 3.5 h over which time, it became cloudy yellow-green in colour. While maintaining the temperature at −78 °C, 2-chloro-1,3,2-dioxaphospholane (1.32 mL, 14.9 mmol, 2.2 equiv.) was added dropwise by syringe to generate a cloudy brown coloured solution. The mixture was allowed to slowly warm to ambient temperature with stirring over 21.5 h, over which time it acquired a cloudy yellow appearance. *Note*: following this point, all procedures for the preparation of **4** do not require the use of dry solvent, but the solvent must be thoroughly degassed prior to use and inert atmosphere conditions must be maintained. The reaction mixture was diluted with Et_2O (250 mL), quenched with degassed water (100 mL) and vigorously mixed. The aqueous layer was removed by cannula and the organic layer was dried over $MgSO_4$. The ether solution was filtered and all volatile components were removed from the flask under reduced pressure to yield **4** as a solid yellow residue. Yield: 2.94 g (92%). ^{1}H NMR (benzene-d_6): δ 7.54 (s, 2H, Cz C*H*), 7.42 (s, 2H, Cz C*H*), 3.49 (m, 4H, $PO_2(CH_2)_2$), 3.16 (m, 4H m, 4H, $PO_2(CH_2)_2$), 2.24 (s, 6H, Cz CH_3), 1.60 (s, 9H, $OC(CH_3)_3$). ^{13}C{^{1}H} NMR (chloroform-*d*): δ 152.8 (s, OC=O), 138.7 (d, J_{CP} = 5.6 Hz, Cz *ipso-C*), 133.6 (s, Cz *ipso-C*), 132.1 (d, J_{CP} = 63.1 Hz, Cz 1,8-*C*), 129.3 (d, J_{CP} = 16.3 Hz, Cz 2,7-*C*H), 126.7 (s, Cz *ipso-C*), 120.9 (s, Cz 4,5-*C*H), 87.2 (s, $OC(CH_3)_3$), 64.3 (d, J_{CP} = 9.5 Hz, $PO_2(CH_2)_2$), 28.6 (t, J_{CP} = 3.3 Hz, $OC(CH_3)_3$), 21.3 (s, Cz CH_3). ^{31}P{^{1}H} NMR (benzene-d_6): δ 148.7. Anal. Calcd (%) for $C_{23}H_{27}NO_6P_2$: C, 58.11; H, 5.72; N, 2.95. Found: C, 57.99; H, 5.53; N, 3.10.

Synthesis of 5

A 250 mL bomb was charged with a suspension of **4** (2.94 g, 6.18 mmol) in toluene (50 mL) and placed under static vacuum. The cloudy orange suspension was heated to 160 °C for 1.5 h, over which time the colour changed to pale orange-yellow. While still hot, the mixture was transferred by cannula to a 100 mL round-bottomed flask and the volatile components were removed under vacuum to afford a yellow residue. In a glove box, the product was suspended in 3 mL of toluene, heated to dissolve all material and then very slowly cooled back to ambient temperature to recrystallize. Pure pale yellow crystals of **5** were collected by filtration, washed with a minimal amount of cold pentane and thoroughly dried under reduced pressure. Yield: 1.56 g (67%). ^{1}H NMR (benzene-d_6): δ 9.95 (br s, 1H, N*H*), 7.76 (s, 2H, 4,5-Cz C*H*), 7.35 (d, $^3J_{HP}$ = 7.0 Hz, 2H, 2,7-Cz C*H*), 3.45 (m, 8H, $PO_2(CH_2)_2$), 2.34 (s, 6H, 3,6-Cz CH_3). ^{13}C{^{1}H} NMR (chloroform-*d*): δ 137.6 (d, J_{CP} = 7.0 Hz, Cz *ipso-C*), 128.8 (d, J_{CP} = 3.9 Hz, Cz *ipso-C*), 127.5 (d, J_{CP} = 20.5 Hz, Cz 2,7-*C*H), 123.9 (d, J_{CP} = 48.4 Hz, Cz 1,8-*C*), 122.8 (s, Cz *ipso-C*), 122.2 (s, Cz 4,5-*C*H), 65.0 (d, J_{CP} = 9.0 Hz, $PO_2(CH_2)_2$), 21.4 (s, Cz CH_3). ^{31}P{^{1}H} NMR (benzene-d_6): δ 167.9. Anal. Calcd (%) for $C_{18}H_{19}NO_4P_2$: C, 57.61; H, 5.10; N, 3.73. Found: C, 58.01; H, 5.16; N, 3.67.

Synthesis of 6

A 100 mL round-bottomed flask was charged with **5** (1.05 g, 2.80 mmol, 1 equiv.) and 40 mL of toluene to give a yellow suspension. At ambient temperature, *para*-isopropylphenyl azide (0.904 g, 5.61 mmol, 2 equiv.) was added dropwise by syringe and the mixture was stirred at ambient temperature for 2 h. As the reaction progressed, the slow evolution of N_2 gas occurred with bubbling and the reaction mixture gradually clarified to give a clear yellow solution. All volatile components were removed under reduced pressure to afford a solid yellow residue. The product was taken up in boiling toluene (10 mL) and cooled very slowly to ambient temperature to recrystallize. Yellow crystals of the product were collected by filtration, washed with cold pentane and thoroughly dried under reduced pressure. Yield: 1.32 g (73%). ^{1}H NMR (benzene-d_6): δ 12.0 (br s, 1H, N*H*), 7.76 (s, 2H, 4,5-Cz C*H*), 7.69 (d, $^3J_{HP}$ = 16.2 Hz, 2H, 2,7-Cz C*H*), 7.41 (dd, $^3J_{HH}$ = 8.4 Hz, $^4J_{HP}$ = 2.5 Hz, 2H, 2,6-Pipp C*H*), 7.11 (dd, $^3J_{HH}$ = 8.2 Hz, $^5J_{HP}$ = 1.5 Hz, 2H, 3,5-Pipp C*H*), 3.56 (m, 8H, $PO_2(CH_2)_2$), 2.84 (sp, $^3J_{HH}$ = 6.9 Hz, 2H,

Pipp C*H*(CH$_3$)$_2$), 2.31 (s, 6H, Cz C*H*$_3$), 1.27 (d, $^3J_{HH}$ = 6.9 Hz, 12H, Pipp CH(C*H*$_3$)$_2$). ^{13}C{^{1}H} NMR (chloroform-*d*): δ 144.4 (d, J_{CP} = 8.2 Hz, Pipp *ipso-C*), 140.5 (d, J_{CP} = 3.2 Hz, Pipp *ipso-C*), 139.5 (d, J_{CP} = 5.4 Hz, Cz *ipso-C*), 130.5 (d, J_{CP} = 9.0 Hz, Cz 4,5-*C*H), 128.1 (d, J_{CP} = 15.1 Hz, Cz *ipso-C*), 126.7 (s, Pipp 3,5-*C*H), 125.1 (d, J_{CP} = 3.2 Hz, Cz 2,7-*C*H), 124.2 (d, J_{CP} = 16.3 Hz, Pipp 2,6-*C*H), 123.5 (d, J_{CP} = 12.6 Hz, Cz *ipso-C*), 108.2 (d, J_{CP} = 202.9 Hz, Cz *ipso-C*), 66.3 (s, PO$_2$(*C*H$_2$)$_2$), 33.3 (s, Pipp *C*H(CH$_3$)$_2$), 24.2 (s, Pipp CH(*C*H$_3$)$_2$), 21.3 (s, Cz *C*H$_3$). ^{31}P{^{1}H} NMR (chloroform-*d*): δ 25.2. Anal. Calcd (%) for C$_{39}$H$_{44}$N$_3$O$_4$P$_2$ (**6**·0.5 benzene): C, 68.81; H, 6.51; N, 6.17. Found: C, 68.87; H, 6.49; N, 6.04.

Synthesis of 8

In a glove box, a 25 mL Erlenmeyer flask was charged with **6** (0.254 g, 0.395 mmol) and Lu(CH$_2$SiMe$_3$)$_3$(THF)$_2$ (0.231 g, 0.397 mmol). Toluene (5 mL) was added to the flask and the orange reaction mixture was stirred at ambient temperature for 18 h. The solution was gently heated to help solubilize the product and then a hot filtration through bed of Celite was performed. The clear yellow filtrate was concentrated under vacuum to ~1 mL and left at −35 °C to crystallize. Yellow crystals of the product were collected by filtration, washed with a minimal amount of cold pentane and thoroughly dried under reduced pressure. Yield: 0.111 g (28%). ^{1}H NMR (benzene-d_6): δ 8.16 (s, 1H, aromatic C*H*), 8.12 (s, 1H, aromatic C*H*), 8.10 (ov s, 2H, aromatic C*H*), 8.03 (br m, 2H, aromatic C*H*), 7.60–7.20 (ov m, 12H, aromatic C*H*), 7.05 (d, $^3J_{HH}$ = 8.2 Hz, 2H, Pipp C*H*), 6.96 (d, $^3J_{HH}$ = 8.2 Hz, 2H, Pipp C*H*), 5.63 (br s, 2H, aromatic C*H*), 4.69 (m, 2H, C*H*$_2$), 4.53 (m, 1H, C*H*$_2$), 4.33 (m, 1H, C*H*$_2$), 4.03 (m, 1H, C*H*$_2$), 3.82 (ov m, 2H, C*H*$_2$), 3.50 (ov m, 5H, C*H*$_2$), 3.27 (m, 1H, C*H*$_2$), 3.16–2.40 (ov m, 7H, C*H*$_2$ + Pipp C*H*), 2.59 (s, 6H, Cz C*H*$_3$), 2.51 (s, 6H, Cz C*H*$_3$), 2.47 (s, 6H, Cz C*H*$_3$), 2.42 (s, 6H, Cz C*H*$_3$), 1.95–1.42 (ov m, 8H, C*H*$_2$), 1.37 (ov m, 12H, Pipp C*H*$_3$), 1.23 (m, 6H, Pipp C*H*$_3$), 1.15 (m, 6H, Pipp C*H*$_3$), −0.17 (s, 9H, Si(C*H*$_3$)$_3$), −0.21 (s, 9H, Si(C*H*$_3$)$_3$), −0.40 (s, 9H, Si(C*H*$_3$)$_3$), −0.56 (s, 9H, Si(C*H*$_3$)$_3$). ^{13}C{^{1}H} NMR (dichloromethane-d_2): δ 151.9 (d, J_{CP} = 4.3 Hz, aromatic *ipso-C*), 150.7 (d, J_{CP} = 5.3 Hz, aromatic *ipso-C*), 150.6 (d, J_{CP} = 4.7 Hz, aromatic *ipso-C*), 150.4 (d, J_{CP} = 2.4 Hz, aromatic *ipso-C*), 147.9 (d, J_{CP} = 7.2 Hz, aromatic *ipso-C*), 147.8 (d, J_{CP} = 7.2 Hz, aromatic *ipso-C*), 144.4 (d, J_{CP} = 9.4 Hz, aromatic *ipso-C*), 143.9 (d, J_{CP} = 7.9 Hz, aromatic *ipso-C*), 143.4 (d, J_{CP} = 4.1 Hz, aromatic *ipso-C*), 142.4 (ov m, 3 aromatic *ipso-C*), 132.1 (d, J_{CP} = 10.4 Hz, aromatic *C*H), 131.3 (br s, aromatic *C*H), 130.2 (d, J_{CP} = 11.6 Hz, aromatic *C*H), 129.8 (d, J_{CP} = 12.5 Hz, aromatic *C*H), 128.9 (br s, aromatic *C*H), 128.8 (br s, aromatic *C*H), 128.4 (d, J_{CP} = 14.2 Hz, aromatic *C*H), 127.6 (d, J_{CP} = 11.2 Hz, aromatic *C*H), 127.4 (d, J_{CP} = 10.3 Hz, aromatic *ipso-C*), 126.7 (d, J_{CP} = 9.9 Hz, aromatic *ipso-C*), 126.5 (s, aromatic *C*H), 126.1 (d, J_{CP} = 5.4 Hz, aromatic *ipso-C*), 126.0 (d, J_{CP} = 6.2 Hz, aromatic *ipso-C*), 125.9 (s, aromatic *C*H), 125.8 (s, aromatic *C*H), 125.7 (br s, aromatic *C*H), 125.5 (d, J_{CP} = 13.3 Hz, aromatic *ipso-C*), 124.6 (s, aromatic *C*H), 124.5 (s, aromatic *C*H), 124.4 (d, J_{CP} = 3.9 Hz, aromatic *ipso-C*), 124.2 (d, J_{CP} = 3.7 Hz, aromatic *ipso-C*), 124.2 (d, J_{CP} = 14.8 Hz, aromatic *ipso-C*), 124.0 (ov m, 2 aromatic *C*H), 112.7 (d, J_{CP} = 137.3 Hz, aromatic *ipso-C*), 112.3 (d, J_{CP} = 136.4 Hz, aromatic *ipso-C*), 110.7 (d, J_{CP} = 134.1 Hz, aromatic *ipso-C*), 108.9 (d, J_{CP} = 131.7 Hz, aromatic *ipso-C*), 77.5 (d, $^2J_{CP}$ = 10.2 Hz, PO*C*H$_2$CH$_2$O), 76.8 (d, $^2J_{CP}$ = 9.2 Hz, PO*C*H$_2$CH$_2$O), 75.9 (d, $^2J_{CP}$ = 6.7 Hz, PO*C*H$_2$CH$_2$O), 74.0 (d, $^2J_{CP}$ = 7.2 Hz, PO*C*H$_2$CH$_2$O), 67.5 (s, POCH$_2$*C*H$_2$O), 66.7 (s, POCH$_2$*C*H$_2$O), 65.3 (s, POCH$_2$*C*H$_2$O), 64.0 (d, $^3J_{CP}$ = 5.0 Hz, POCH$_2$*C*H$_2$O), 34.0 (m, Pipp *C*H(CH$_3$)$_2$ + Pipp *C*H(CH$_3$)$_2$′ + Pipp *C*H(CH$_3$)$_2$″), 33.6 (s, Pipp *C*H(CH$_3$)$_2$‴), 25.0 (s, Pipp CH-(*C*H$_3$)(CH$_3$)‴), 24.7 (s, Pipp CH(*C*H$_3$)(CH$_3$)′), 24.6–24.5 (m, Pipp CH(*C*H$_3$)$_2$) + Pipp CH(*C*H$_3$)$_2$″), 24.4 (s, Pipp CH(CH$_3$)(*C*H$_3$)′), 23.3 (s, Pipp CH(CH$_3$)(*C*H$_3$)‴), 21.5 (s, Cz *C*H$_3$), 21.4 (s, Cz *C*H$_3$), 21.2 (s, Cz *C*H$_3$), 21.1 (s, Cz *C*H$_3$), 18.3 (d, $^1J_{CP}$ = 92.8 Hz, P*C*H$_2$Si(CH$_3$)$_3$), 14.7 (d, $^1J_{CP}$ = 90.7 Hz, P*C*H$_2$Si(CH$_3$)$_3$), 13.6 (d, $^1J_{CP}$ = 92.1 Hz, P*C*H$_2$Si(CH$_3$)$_3$), 11.0 (d, $^1J_{CP}$ = 84.4 Hz, P*C*H$_2$Si(CH$_3$)$_3$), 0.1 (d, $^3J_{CP}$ = 3.2 Hz, PCH$_2$Si(*C*H$_3$)$_3$), 0.0 (d, $^3J_{CP}$ = 3.1 Hz, PCH$_2$Si(*C*H$_3$)$_3$), −0.4 (d, $^3J_{CP}$ = 3.4 Hz, PCH$_2$Si-(*C*H$_3$)$_3$), −0.5 (d, $^3J_{CP}$ = 3.6 Hz, PCH$_2$Si(*C*H$_3$)$_3$). ^{31}P{^{1}H} NMR (dichloromethane-d_2): δ 55.8 (s, 1P), 54.4 (s, 1P), 48.5 (s, 1P), 48.0 (s, 1P). Anal. Calcd (%) for C$_{93}$H$_{136}$Lu$_2$N$_6$O$_8$P$_4$Si$_4$ (**8**·pentane): C, 54.43; H, 6.68; N, 4.09. Found: C, 54.26; H, 6.32; N, 4.29.

X-ray crystallography

Recrystallization of compound **5** from a concentrated pentane solution at 25 °C, and compounds **6**·0.5 benzene and **8**·pentane from concentrated benzene solutions layered with pentane at 25 °C afforded single crystals suitable for X-ray diffraction. Crystals were coated in dry Paratone oil under an argon atmosphere and mounted onto a glass fibre. Data were collected at −100 °C using a Bruker SMART APEX II diffractometer (Mo Kα radiation, λ = 0.71073 Å) outfitted with a CCD area-detector and a KRYO-FLEX liquid nitrogen vapour cooling device. A data collection strategy using ω and φ scans at 0.5° steps yielded full hemispherical data with excellent intensity statistics. Unit cell parameters were determined and refined on all observed reflections using APEX2 software.[37] Data reduction and correction for Lorentz polarization were performed using SAINT-Plus software.[38] Absorption corrections were applied using SADABS.[39] The structures were solved by direct methods and refined by the least squares method on F^2 using the SHELXTL software suite.[40] All non-hydrogen atoms were refined anisotropically. Hydrogen atom positions were calculated and isotropically refined as riding models to their parent atoms. Table 3 provides a summary of selected data collection and refinement parameters.

Special considerations were required in the refinement of disordered moieties in the structures of **6**·0.5 benzene and **8**·pentane. One dioxaphospholane ring in compound **6** was disordered and the disordered atoms (C15, 52%/C15b, 48%) were refined over two positions, with the use of some distance and displacement restraints. Additionally, geometric restraints were placed on the benzene solvent molecule in **6**·0.5 benzene in order to obtain reasonable bond distances and angles. In the refinement of **8**·pentane, one aromatic ring (C59, 50%/C59b, 50%), three isopropyl groups (C30, 66%/C30b, 34%; C74, 55%/C74b, 45%; C65, 57%/C65b, 43%), one trimethylsilyl group

Table 3 Summary of X-ray crystallography data collection and structure refinement for compounds **5**, **6**·0.5 benzene, and **8**·pentane

	5	**6**·0.5 benzene	**8**·pentane[a]
Formula	$C_{18}H_{19}NO_4P_2$	$C_{39}H_{44}N_3O_4P_2$	$C_{93}H_{136}Lu_2N_6O_8P_4Si_4$
Fw/g mol^{-1}	375.28	680.71	2052.26
Cryst syst	Triclinic	Orthorhombic	Triclinic
Space group	$P\bar{1}$	*Pbca*	$P\bar{1}$
a/Å	8.3969(9)	10.3386(7)	14.763(5)
b/Å	10.2686(10)	20.4403(13)	18.123(6)
c/Å	10.6756(11)	32.986(2)	19.174(6)
α/°	93.7620(10)	90	80.777(4)
β/°	111.3110(10)	90	84.329(4)
γ/°	93.6660(10)	90	83.766(4)
Volume/Å^3	851.88(15)	6970.8(8)	5016(3)
Z	2	8	2
D_{calc}/mg m^{-3}	1.463	1.297	1.359
μ/mm^{-1}	0.279	0.170	2.122
Cryst size/mm	0.17 × 0.17 × 0.03	0.47 × 0.42 × 0.08	0.20 × 0.06 × 0.03
Cryst colour	Colourless	Colourless	Yellow
Cryst habit	Plate	Prism	Prism
θ range/°	2.00 to 27.10	1.99 to 27.10	1.69 to 26.37
N	11 666	75 247	54 488
N_{ind}	3735	7693	20 429
Data/restraints/parameters	3735/0/228	7693/5/458	20 429/209/1083
GoF on F^2	1.021	1.053	0.916
R_1 ($I > 2\sigma(I)$)[b]	0.0374	0.0382	0.0457
wR_2 ($I > 2\sigma(I)$)[c]	0.0905	0.0986	0.0884
R_1 (all data)[b]	0.0523	0.0475	0.0814
wR_2 (all data)[c]	0.0980	0.1054	0.0988
$\Delta\rho_{max}$ and $\Delta\rho_{min}$/e Å^{-3}	0.360 and −0.311	0.362 and −0.358	0.582 and −0.844

Notes: [a] Crystallized with a highly disordered molecule of pentane in the asymmetric unit, which was removed from the reflection file using the SQUEEZE subroutine of PLATON. [b] $R_1 = \sum||F_o| - |F_c||/\sum|F_o|$. [c] $wR_2 = \{\sum[w(F_o^2 - F_c^2)^2]/\sum[w(F_o^2)^2]\}^{1/2}$.

(Si2, 58%/Si2b, 42%) and the pentane solvent molecule were disordered. Disordered atoms in **8** were refined over two positions and some restraints (geometric and displacement) were applied. No suitable disorder model could be found for the severely disordered pentane molecule. The electron density associated with the pentane molecule was removed from the reflection file using the SQUEEZE subroutine of the PLATON program.[41]

Acknowledgements

This research was financially supported by the Natural Sciences and Engineering Research Council (NSERC) of Canada and the Canada Foundation for Innovation (CFI).

References

1 W. E. Piers and D. J. H. Emslie, *Coord. Chem. Rev.*, 2002, **233–234**, 131–155.
2 P. Mountford and B. D. Ward, *Chem. Commun.*, 2003, 1797–1803.
3 F. T. Edelmann, D. M. M. Freckmann and H. Schumann, *Chem. Rev.*, 2002, **102**, 1851–1896.
4 J. D. Masuda, K. C. Jantunen, O. V. Ozerov, K. J. T. Noonan, D. P. Gates, B. L. Scott and J. L. Kiplinger, *J. Am. Chem. Soc.*, 2008, **130**, 2408–2409.
5 E. Lu, Y. Li and Y. Chen, *Chem. Commun.*, 2010, **46**, 4469–4471.
6 J. Chu, E. Lu, Z. Liu, Y. Chen, X. Leng and H. Song, *Angew. Chem., Int. Ed.*, 2011, **50**, 7677–7680.
7 E. Lu, J. Chu, Y. Chen, M. V. Borzov and G. Li, *Chem. Commun.*, 2011, **47**, 743–745.
8 E. Lu, Q. Zhou, Y. Li, J. Chu, Y. Chen, X. Leng and J. Sun, *Chem. Commun.*, 2012, **48**, 3403–3405.
9 T. K. Panda and P. W. Roesky, *Chem. Soc. Rev.*, 2009, **38**, 2782–2804.
10 P. W. Roesky, *Z. Anorg. Allg. Chem.*, 2006, **632**, 1918–1926.
11 R. G. Cavell, R. P. Kamalesh Babu and K. Aparna, *J. Organomet. Chem.*, 2001, **617–618**, 158–169.
12 S. T. Liddle, D. P. Mills and A. J. Wooles, *Chem. Soc. Rev.*, 2011, **40**, 2164–2176.
13 N. D. Jones and R. G. Cavell, *J. Organomet. Chem.*, 2005, **690**, 5485–5496.
14 J. D. Masuda, P. Wei and D. W. Stephan, *Dalton Trans.*, 2003, 3500–3505.
15 D. Li, S. Li, D. Cui, X. Zhang and A. A. Trifonov, *Dalton Trans.*, 2011, **40**, 2151–2153.
16 D. Li, S. Li, D. Cui and X. Zhang, *J. Organomet. Chem.*, 2010, **695**, 2781–2788.
17 G. C. Welch, W. E. Piers, M. Parvez and R. McDonald, *Organometallics*, 2004, **23**, 1811–1818.
18 B. Liu, D. Cui, J. Ma, X. Chen and X. Jing, *Chem.–Eur. J.*, 2007, **13**, 834–845.

19 B. Liu, X. Liu, D. Cui and L. Liu, *Organometallics*, 2009, **28**, 1453–1460.
20 K. D. Conroy, W. E. Piers and M. Parvez, *J. Organomet. Chem.*, 2008, **693**, 834–846.
21 W. Rong, D. Liu, H. Zuo, Y. Pan, Z. Jian, S. Li and D. Cui, *Organometallics*, 2013, **32**, 1166–1175.
22 K. R. D. Johnson and P. G. Hayes, *Organometallics*, 2009, **28**, 6352–6361.
23 K. R. D. Johnson and P. G. Hayes, *Organometallics*, 2013, **32**, 4046–4049.
24 K. R. D. Johnson, M. A. Hannon, J. S. Ritch and P. G. Hayes, *Dalton Trans.*, 2012, **41**, 7873–7875.
25 T.-P.-A. Cao, A. Buchard, X. F. Le Goff, A. Auffrant and C. K. Williams, *Inorg. Chem.*, 2012, **51**, 2157–2169.
26 C. Bakewell, T.-P.-A. Cao, X. F. Le Goff, N. J. Long, A. Auffrant and C. K. Williams, *Organometallics*, 2013, **32**, 1475–1483.
27 K. R. D. Johnson and P. G. Hayes, *Chem. Soc. Rev.*, 2013, **42**, 1947–1960.
28 A. B. Burg and P. J. Slota Jr., *J. Am. Chem. Soc.*, 1960, **82**, 2148–2151.
29 H. Hacklin and G.-V. Röschenthaler, *Phosphorus Sulfur*, 1988, **36**, 165–169.
30 G. J. P. Britovsek, V. C. Gibson, O. D. Hoarau, S. K. Spitzmesser, A. J. P. White and D. J. Williams, *Inorg. Chem.*, 2003, **42**, 3454–3465.
31 K. Smith, D. M. James, A. G. Mistry, M. R. Bye and D. J. Faulkner, *Tetrahedron*, 1992, **48**, 7479–7488.
32 K. R. D. Johnson and P. G. Hayes, *Organometallics*, 2011, **30**, 58–67.
33 J. Cámpora and S. L. Buchwald, *Organometallics*, 1993, **12**, 4182–4187.
34 H. Schumann, D. M. M. Freckmann and S. Dechert, *Z. Anorg. Allg. Chem.*, 2002, **628**, 2422–2426.
35 F. Estler, G. Eickerling, E. Herdtweck and R. Anwander, *Organometallics*, 2003, **22**, 1212–1222.
36 S. Arndt, P. Voth, T. P. Spaniol and J. Okuda, *Organometallics*, 2000, **19**, 4690–4700.
37 *APEX2*, Bruker AXS, Madison, WI, 2010.
38 *SAINT-Plus*, Bruker AXS, Madison, WI, 2009.
39 G. M. Sheldrick, *SADABS*, Bruker AXS, Madison, WI, 2008.
40 G. M. Sheldrick, *Acta Crystallogr., Sect. A: Found. Crystallogr.*, 2007, **64**, 112–122.
41 A. L. Spek, *J. Appl. Crystallogr.*, 2003, **36**, 7–13.